Markov Processes Relat. Fields **26**, 167–183 (2020)

Markov Processes and **Related Fields**

The Non-Equilibrium Ising Model in Two Dimensions: a Numerical Study

Cristian Giardinà

University of Modena and Reggio Emilia, via G. Campi 213/b, 41125 Modena, Italy

Received March 11, 2019

Abstract. In this paper, we study the boundary-driven ferromagnetic Ising model in two dimensions. In this non-equilibrium setting, in the low temperature region, the Ising model has phase separation in the presence of a current. We investigate, by means of numerical simulations, Kawasaki dynamics with magnetization reservoirs. The results show that, in the stationary non-equilibrium state, the Ising model may have uphill diffusion and magnetization profiles with three discontinuities. These results complement the results of a previous paper by Colangeli, Giberti, Vernia and the present author [9]. They also allow to state a full picture of the hydrodynamic limit.

Keywords: 2D Ising model, non-equilibrium statistical mechanics

AMS Subject Classification: 82C22

1. Introduction and outline

In this contribution we discuss the *boundary driven Ising model in two dimensions*. From the statistical physics perspective, it is very natural to consider this system. Indeed, the *closed* Ising model (for instance with periodic boundary conditions) is the main mathematical model to describe the phenomenon of a second-order phase transition occurring at inverse critical temperature $0 < \beta_c < \infty$ [23, 26]. In the equilibrium setting the two-dimensional ferromagnetic Ising model turns out to be exactly solvable, with beautiful mathematical structures arising from integrability [2]. Here, we will be interested in studying the *open* Ising model, driven into a non-equilibrium states by imposing different magnetization values at two boundaries.

More precisely, we shall consider the following setting, which is schematically depicted in Figure 1.

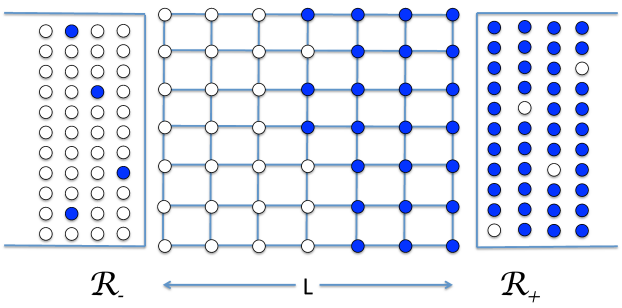

Figure 1. Schematic picture of the boundary driven 2D Ising model.

In the bulk, the spins (that can also be read as particles via the standard mapping to lattice gases) interact as in the nearest neighbors two-dimensional ferromagnetic Ising model on a square lattice with $L \times L$ sites ($L \in \mathbb{N}$) and they evolve following a Kawasaki dynamics at inverse temperature $0 \leq \beta < \infty$. At the opposite boundaries in the horizontal direction, infinite reservoirs $\mathcal{R}_-$ and $\mathcal{R}_+$ fix the magnetizations to values $-1 \leq m_- \leq 1$ and $-1 \leq m_+ \leq 1$ by means of two independent spin-flip dynamics with different parameters. This set-up typically forces a magnetization current through the system and one is interested in the structure of the stationary measure (as a function of the reservoirs magnetizations $m_\pm$). The focus of this paper is on the low temperature regime (i.e. the bulk Kawasaki dynamics occurs at inverse temperature β higher that the critical value β_c), where phase separation occurs for positive m_+ and negative m_-. We shall especially be concerned with the expected value of the current in the non-equilibrium steady state and the verification of Fick's law which, in our setting, states the proportionality between the average current and the negative of the gradient of the magnetization. For the boundary driven Ising model no closed form is known for the non-equilibrium invariant measure (not even in one dimension).

The paper is organized as follows. In the next section we define the model via its Markov generator. In Section 3 we state the conjectured hydrodynamic limit, i.e. the diffusive scaling limit of empirical magnetization. Section 4 contains the main results on the measurements of current and magnetization profiles, whereas Section 5 is focused on the finite-size effects, that play a crucial role in such measurements. Finally, in the last section we draw some conclusions.

2. Set up: model definition

We consider a subset Λ_L of the two-dimensional lattice: $\Lambda_L = [1, L]^2 \cap \mathbb{Z}^2$. Sites of this finite volume are denoted by the vector $i = (x, y)$. To each site $i \in \Lambda_L$ we associate a dichotomic spin variable $\sigma_i \in \{-1, 1\}$. We shall consider the continuous time Markov process $\{\sigma(t)\ , t \geq 0\}$ with state space $\Omega_L := \{-1, 1\}^{L^2}$, where the i^{th} component $\sigma_i(t)$ denotes the value of spin at site $i \in \Lambda$ at time $t \geq 0$. The process is defined by its generator $\mathcal{L}$, working on functions $f : \Omega_L \to \mathbb{R}$, which is the sum of three terms:

$$\mathcal{L}f(\sigma) = \mathcal{L}_- f(\sigma) + \mathcal{L}_b f(\sigma) + \mathcal{L}_+ f(\sigma). \tag{2.1}$$

We now describe the three contributions. The bulk term $\mathcal{L}_b$ reads

$$\mathcal{L}_b f(\sigma) = \sum_{i \sim j \in \Lambda_L} c(i, j; \sigma)[f(\sigma^{i,j}) - f(\sigma)], \tag{2.2}$$

where $i \sim j$ denotes that the sites i and j are nearest neighbors and $\sigma^{i,j}$ denotes the spin configuration with components

$$\sigma_k^{i,j} = \begin{cases} \sigma_k & \text{if } k \neq i, j \\ \sigma_j & \text{if } k = i \\ \sigma_i & \text{if } k = j. \end{cases}$$

In words, the Markov process generated by $\mathcal{L}_b$ is described as follows: on the $2L^2$ edges of Λ_L connecting nearest neighbors sites there are independent exponential clocks; if the clock of the bond (i, j) rings first, then the spins σ_i and σ_j are exchanged. After the exchange the clocks are reset and the procedure is repeated. The clock rates $c(i, j; \sigma)$ are those of the Kawasaki dynamics

$$c(i, j; \sigma) = \mathbf{1}_{\sigma_i \neq \sigma_j} \cdot \begin{cases} 1 & \text{if } \Delta H(\sigma) = H_L(\sigma^{i,j}) - H_L(\sigma) \leq 0 \\ e^{-\beta \Delta H(\sigma)} & \text{otherwise,} \end{cases} \tag{2.3}$$

with H_L the finite-volume Hamiltonian of the 2D nearest neighbors ferromagnetic Ising model

$$H_L(\sigma) = -\sum_{x=1}^{L} \sum_{y=1}^{L} \sigma_{(x,y)} \sigma_{(x,y+1)} - \sum_{x=0}^{L} \sum_{y=1}^{L} \sigma_{(x,y)} \sigma_{(x+1,y)}. \tag{2.4}$$

In the above formula, the first double sum is over vertical bonds, where we assume periodic boundary conditions $\sigma_{(x,L+1)} = \sigma_{(x,1)}$ for $x = 1, \dots L$; the second double sum is over horizontal bonds, where we assume "$L/4$ boundary conditions" [5], i.e. $\sigma_{(0,y)} = \sigma_{(1,y')}$ and $\sigma_{(L+1,y)} = \sigma_{(L,y')}$ where

$$y' \equiv y - \left\lfloor \frac{L}{4} \right\rfloor \pmod{L},$$

with $y = 1, \dots L$, and $\lfloor \cdot \rfloor$ denoting the integer part. Whereas the choice of periodic boundary conditions in the transverse y-direction is the simplest choice that guarantees zero average current in the transverse direction, other choice of the boundary conditions in the x-direction are possible. We made the choice of the "$L/4$ boundary conditions" because this is particularly convenient for the implementation of the numerical simulations. Other choices are discussed in [10], where it is provided convincing arguments that the results that we are going to discuss essentially holds true for a wide class of choices that break detailed balance at the boundaries.

The generators $\mathcal{L}_\pm$ are given by

$$\mathcal{L}_\pm f(\sigma) = \sum_{i \in \Lambda_\pm} c_\pm(i, \sigma)[f(\sigma^i) - f(\sigma)], \tag{2.5}$$

where the boundaries $\Lambda_{\pm,L}$ are defined as

$$\Lambda_{-,L} = \{(1, y) \in \Lambda \ : \ y = 1, \dots, L\},$$

$$\Lambda_{+,L} = \{(L, y) \in \Lambda \ : \ y = 1, \dots, L\},$$

and σ^i denotes the spin configuration with components

$$\sigma^i_k = \begin{cases} \sigma_k & \text{if } k \neq i \\ -\sigma_i & \text{if } k = i. \end{cases}$$

Thus on the L bonds connecting the boundary $\Lambda_{-,L}$ to the left reservoir there are independent exponential clocks; if the clock of the site $(1, y)$ rings first then the spin $\sigma_{(1,y)}$ is flipped. A similar process occurs on the right boundary $\Lambda_{+,L}$ and the two processes are independent. The rates of these spin-flip dynamics

$$c_\pm(i; \sigma) = \frac{1 - \sigma_i m_\pm}{2}$$

are such that on the sites of the left boundary, resp. right boundary, an average magnetization m_-, resp. m_+, is fixed. In the following we will assume (unless otherwise stated) that the boundary magnetizations are $m_- = -m_+$. This implies that the stationary magnetization profile is symmetric with respect to $x = \lfloor L + 1 \rfloor / 2$. Without loss of generality we can also restrict to $0 \leq m_+ \leq 1$.

We recall that the equilibrium Ising model in two dimension with Hamiltonian (2.4) has, in the thermodynamic limit $L \to \infty$, a second order phase transition at inverse critical temperature

$$\beta_c = \frac{\ln(1 + \sqrt{2})}{2} \approx 0.440686.$$

The order parameter is provided by the spontaneous magnetization, which is defined as

$$m_\beta = \lim_{B \searrow 0} \lim_{L \to \infty} \sum_{\sigma \in \Omega_L} \Big(\frac{1}{L^2} \sum_{i \in \Lambda_L} \sigma_i \Big) \frac{\exp\{-\beta H_L(\sigma) + B \sum_{i \in \Lambda_L} \sigma_i\}}{Z_L(\beta, B)}.$$

In the above formula it is understood that the Hamiltonian H_L has periodic boundary conditions in all directions and Z_L is the normalizing partition function. The exact solution of the equilibrium 2D Ising model [23, 26] gives

$$m_\beta = \begin{cases} 0 & \text{if } \beta \leq \beta_c \\ \left[1 - \sinh^{-4}(2\beta)\right]^{1/8} & \text{if } \beta > \beta_c \end{cases}$$

and the spontaneous magntization is shown in Figure 2.

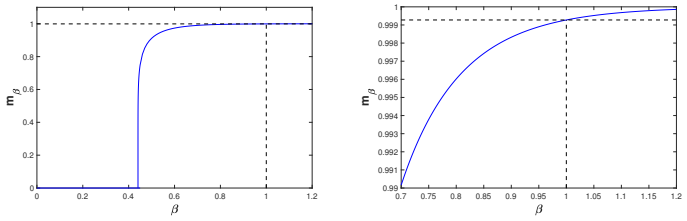

Figure 2. Spontaneous magnetization m_β of the equilibrium 2D Ising model as a function of the inverse temperature β (left panel), with a zoom around the value $\beta = 1$ that is used in the numerical simulations (right panel).

We will be interested in studying the boundary driven Ising model in two dimension as the following two parameters are varied:

- the bulk temperature $0 \leq \beta < \infty$,
- the boundary magnetization $0 \leq m_+ \leq 1$.

For reasons that will become clear in the following sections we shall call *stable* the region in the parameter space such that $\beta \geq \beta_c$ and $m_+ > m_\beta$ and *unstable* the region where $\beta \geq \beta_c$ and $m_+ < m_\beta$. Possibly, at finite volume, there will also be a *metastable* region separating the stable and the unstable regions.

3. Hydrodynamics

A rigorous study of the hydrodynamics (large space-time scale) is currently not available for the model described in the previous section. We discuss here the heuristic guess of the hydrodynamic picture and mention some of the problems

one has to solve (work in progress with A. De Masi and E. Presutti). We assume that the starting configuration $\sigma(0)$ is distributed according to a sequence of initial measure $\mu^{(L)}$ on Ω_L such that

$$\lim_{L\to\infty} \frac{1}{L^2} \sum_{i\in\Lambda_L} \phi\Big(\frac{i}{L}\Big)\sigma_i(0) = \int_{[0,1]^2} \phi(r)M_0(r)dr$$

where $\phi : \mathbb{R}^2 \to \mathbb{R}$ is a test function and $M_0 : [0,1]^2 \to [-1,1]$ is the starting macroscopic magnetization profile. This convergence has to be understood as convergence in probability w.r.t the initial measure $\mu^{(L)}$. We consider the diffusive scaling of the the empirical magnetization field. Then the *hydrodynamic limit* holds if

$$\lim_{L\to\infty} \frac{1}{L^2} \sum_{i\in\Lambda_L} \phi\Big(\frac{i}{L}\Big)\sigma_i(L^2t) = \int_{[0,1]^2} \phi(r)M(r,t)dr$$

where $M(\cdot,t) : [0,1]^2 \to [-1,1]$ is the macroscopic magnetization profile at time $t > 0$. Again the convergence is understood in probability, now with respect to the law $\mu_t^{(L)}$ of the process at time L^2t.

There are two regimes where one can state the conjectured evolution of the magnetization profile: in the high temperature region it is the solution of the *non-linear heat equation* with Dirichlet boundary condition; in the low-temperature stable region it is associated to the solution of a *free boundary problem*. More precisely one expects the following:

1. **High temperature region:** $0 \le \beta < \beta_c$. In this regime there is no phase separation. By the the choice of periodic boundary conditions in the vertical direction, we have that if we start from an initial macroscopic profile that is a function of the sole horizontal macroscopic coordinate, i.e. $M_0(r) = m_0(r_1)$ with $r_1 \in [0,1]$, then $M(r,t) = m(r_1,t)$ is the unique solution of:

$$\begin{aligned} &\frac{\partial m}{\partial t} = \frac{\partial}{\partial r_1}\left(D(m)\frac{\partial m}{\partial r_1}\right), \\ &m(0,t) = -m_+, \qquad m(1,t) = m_+, \\ &m(r_1,0) = m_0(r_1) \end{aligned} \tag{3.1}$$

   with $D(m) > 0$ the bulk diffusion coefficient calculated from the Green–Kubo formula (see eq. (2.6) in [25]).

2. **Low temperature regime:** $\beta > \beta_c$. In this regime we expect phase-coexistence with regions (interfaces) where the magnetization profile is not slowly varying. We further assume, besides the vertical symmetry $M_0(r) = m_0(r_1)$, that the starting measure is such that the initial macroscopic

profile has only one interface. Then at later time $t > 0$ there is also a unique interface and, calling $R_t \in [0,1]$ its position, we have that the couple $(m(r_1,t), R_t)$ is the unique solution of the free boundary problem:

$$\begin{aligned}
\frac{\partial m}{\partial t} &= \frac{\partial}{\partial r_1}\left(D(m)\frac{\partial m}{\partial r_1}\right), \qquad r_1 \in [0,R_t)\cup(R_t,1], \quad (3.2)\\
m(0,t) &= -m_+, \qquad m(R_t^-,t) = -m_\beta,\\
m(R_t^+,t) &= m_\beta, \qquad m(1,t) = m_+,\\
2m_\beta\frac{dR_t}{dt} &= -D(m_\beta)\frac{\partial m}{\partial r_1}(R_t^+,t) + D(-m_\beta)\frac{\partial m}{\partial r_1}(R_t^-,t),\\
m(r_1,0) &= m_0(r_1).
\end{aligned}$$

The following comments are in order:

i) At infinite temperature $\beta = 0$, the process with generator (2.1) degenerates to the symmetric exclusion process, with a constant bulk diffusivity so that (3.1) becomes the linear heat equation with Dirichlet boundary conditions [12].

ii) In the low temperature region $\beta > \beta_c$, Spohn and Yau [25] have proved that bulk diffusivity satisfies

$$D(m) > 0 \quad \text{if } |m| \geq m_\beta, \qquad D(m) = 0 \ \text{ otherwise.}$$

iii) To prove (3.1) or (3.2), one needs substantial improvements of the standard approaches that are currently available to derive the hydrodynamic limit. Indeed the duality method [12] does not apply to the hierarchy of correlation functions, whereas the entropy method [15,27] needs to be extended to cover systems with phase transitions and reservoirs. Along these lines, [16] considers discrete lattice gas models in a finite interval with reversible stochastic dynamics at the boundaries, however the assumption on the jumps rates of the bulk stochastic dynamics exclude the possibility of phase transitions; [22] studies a system of interacting diffusions (Ginzburg-Landau with a potential) with periodic boundary conditions, including the possibility of a phase transition. However the inclusion of reservoirs in the context of unbounded state space is not straightforward since one does not have a full control of entropy production at the boundaries.

iv) Both in the high temperature regime and in the low temperature stable regime with $m_+ > m_\beta$, we expect Fick's law to be satisfied in the stationary state. The stationary magnetization profile $m : [0,1] \to [-1,1]$ should have the shape depicted in Figure 3 (left and central panels).

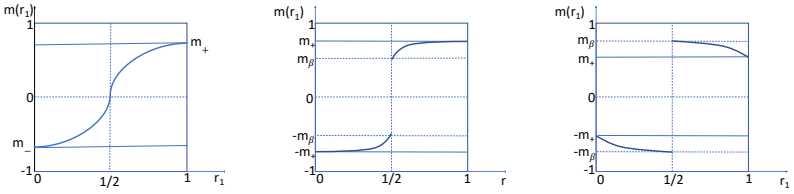

Figure 3. Stationary macroscopic magnetization profile $m(r_1)$ in the high temperature region (left panel) and in the low temperature stable regime with $m_+ > m_\beta$ (central panel). The profile in the right panel is **unstable** in the low temperature region with $m_+ < m_\beta$ and thus will never be reached by the dynamics.

In the high temperature region (left panel) the stationary magnetization profile continuously interpolate from $-m_+$ and m_+, whereas in the low temperature stable regime with $m_+ > m_\beta$ (central panel) it has a jump (of size $2m_\beta$) at $r_1 = 1/2$, which is the stationary location of the interface. The current $J = -D(m)\frac{dm}{dr_1}$ is negative: the magnetization is transported from the right boundary with higher magnetization to the left boundary with lower magnetization.

A naive guess for the stationary solution in the low temperature regime with $m_+ < m_\beta$ would be the one depicted on the right panel of Fig. 3. However, a simple reasoning on the stability of this profile with respect to small displacement of the interface, immediately entails that such profile is unstable and thus will never be reached by the dynamics. We shall see in Section 4.2 the actual shape of the magnetization profile in this regime, and explain it on the base of finite size effects in Section 5.

4. Main results of numerical simulations

By means of Monte Carlo simulations, we first verify the hydrodynamic picture in the low temperature stable region with $m_+ > m_\beta$ and then we investigate the behavior of the system in the low temperature unstable region with $m_+ < m_\beta$, for which it is hard to formulate a conjecture. For the sake of space we do not show results in the high-temperature region.

As in [9], we focus on the current and the magnetization profile in the stationary state. In the numerical simulations these quantities can be estimated by means of temporal averages. We thus simulated the Markov process with generator (2.1) generating long trajectories. We have fixed the inverse temperature $\beta = 1$ and varied the system size L (up to $L = 40$) and the boundary mag-

netizations m_+ (around the spontaneous magnetization $m_{|_{\beta=1}} = 0.9992757$). We always used $m_- = -m_+$ and periodic boundary conditions in the vertical direction and "$L/4$ boundary conditions" in the horizontal direction. We tried several different initial conditions, for instance random, or instanton-like (i.e., $\sigma_{(x,y)} = -1$ for $x \in [1, L/2]$ and $\sigma_{(x,y)} = 1$ for $x \in (L/2, L]$), checking that the results do not depend on the choice of the starting spin configuration.

4.1. Current

The current in the stationary state can be estimated with the following temporal average:

$$J = \lim_{T\to\infty} \frac{J_{x,y}(T)}{T} \qquad \forall\ (x,y) \in \Lambda,$$

where $J_{x,y}(T)$ is the current up to time T between (x,y) and $(x+1,y)$, i.e. the number of positive spins that, in the time interval $[0,T]$, have crossed an horizontal bond from left to right minus the number of positive spins that have crossed the bond in the opposite direction. We checked that, as it should be, the current is the same – within numerical accuracy – on each horizontal bond.

The result for the stationary current is illustrated in Fig. 4.

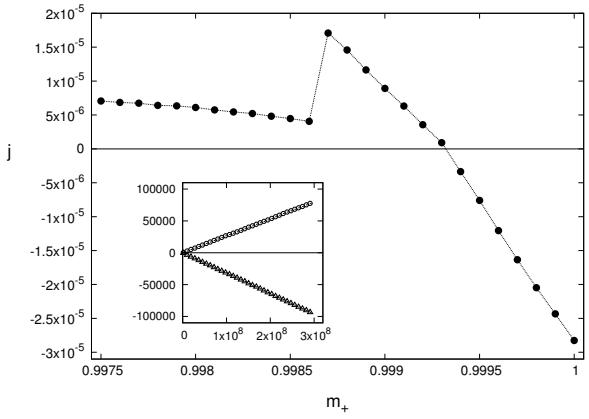

Figure 4. Current vs. reservoir magnetization for system size $L = 40$. Each data point is the current J measured in the non-equilibrium stationary state with a given value m_+ on the right reservoir $\mathcal{R}_+$ and $m_- = -m_+$ on the left reservoir $\mathcal{R}_-$. The inset shows the integrated current up to time $T = 3 \times 10^8$ steps for $m_+ = 0.9995$ (negative slope) and for $m+ = 0.99910$ (positive slope).

There it is plotted the current J as a function of the right reservoir magnetization m_+, which varies in the interval $[0.9975, 1]$ in steps of 10^{-4}. Such a

narrow interval is due to the value of the spontaneous magnetization at $\beta = 1$ ($m_{\beta=1} \approx 0.99927$) and finite size corrections that are of order $L^{-2/5}$ [14]. The current has to be measured over a sufficiently long time span to get rid of fluctuations and to ensure the convergence to the stationary regime. This can be tested by monitoring the running average of the current and looking at the scale of its fluctuations. As a result, we have verified that 10^{12} spin exchanges are needed to guarantee relative fluctuations of 1% in the worst cases. In Fig. 4 errors bars are smaller than the size of the points.

From Fig. 4 we see the existence of a critical value $m_{crit} \approx 0.99931$ such that:

- if $m_+ > m_{crit}$ then the current is negative,
- if $m_+ < m_{crit}$ the current is positive.

To let better appreciate the change of sign we plot in the inset the integrated current up to time $T = 3 \times 10^8$ steps. We see that for $m_+ = 0.99950$ there is a straight line with a negative slope, whereas for $m+ = 0.99910$ we measure a positive slope.

Thus, numerical simulations verify the hydrodynamic prediction of a negative current in the low temperature stable regime with $m_+ > m_\beta$. Surprisingly, they yield instead a positive *uphill* current in the low temperature unstable regime with $m_+ < m_\beta$: magnetization flows from the left to the right reservoir. Some theoretical evidence of this intriguing physical phenomenon was recently reported in [6–8, 13] for 1D particle systems with Kac potentials (where phase transitions are obtained in a mean-field limit).

We also remark that the critical value m_{crit} is very close to the spontaneous magnetization (the difference being on the forth decimal digit). The dependence of $m_{crit}(L)$ from the linear system size L has been investigated in [9]. There it has been found (using the argument that the zero of the current can be associated to the equilibrium setting) that $m_{crit}(L)$ approaches m_β exponentially fast.

4.2. Magnetization profile

The magnetization profile in the stationary state can be estimated with the following temporal average:

$$m_x = \lim_{T\to\infty} \frac{1}{T} \int_0^T \left(\frac{1}{L} \sum_{y=1}^{L} \sigma_{(x,y)}(t) \right) dt \qquad\qquad x = 1, \ldots, L$$

We run a simulation with kinetic Monte Carlo method doing 10^{10} spin exchanges and plot in Fig. 5 the time averaged magnetization profiles for three values of the boundary magnetizations.

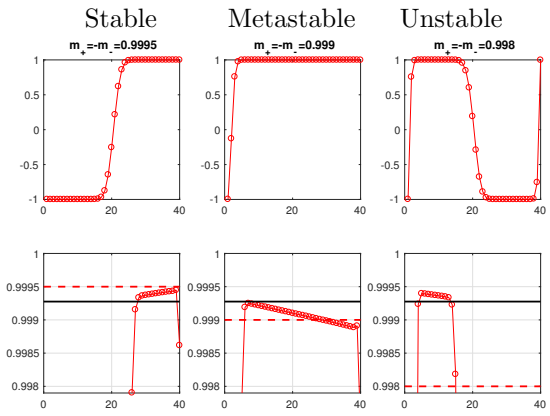

Figure 5. Time-averaged magnetization profiles for three values of the reservoir magnetization: $m_+ = -m_- = 0.9995$ stable phase (left column); $m_+ = -m_- = 0.9990$ meta-stable phase (central column); $m_+ = -m_- = 0.9980$ unstable phase (right column). Bottom panels provide a zoom on the y-axis. The continuous and dashed lines represent m_β and m_+ respectively.

On the left column, we see that in the low temperature stable regime with $m_+ > m_\beta$ the profile is the finite-volume approximation of the one predicted by hydrodynamics, i.e. an instanton-like profile with a sharp interface at the center. On the central and right columns we show the results for $m_+ < m_\beta$. We see two types of profile: for m_+ slightly less than m_β we have a profile with a bump on the left boundary; for lower m_+ we have a profile with a double bump. In both cases the magnetization at the bump is such that $|m_{bump}| > m_\beta$.

Although surprising at first sight, the profiles that are observed for $m_+ < m_\beta$ are consistent with the current measured in previous subsection. Indeed the zoom in the bottom panels of Fig. 5 shows that the gradient of the magnetization profile (possibly excluding few isolated points that have zero measure in the hydrodynamic limit) has always the opposite sign of the current, in agreement with Fick's law $J = -D(m)\frac{dm}{dr_1}$.

5. Finite-size effects

In this section we further discuss the results of the numerical simulations described above. We shall specifically address the occurrence of the profile with one bump. The aim is to provide quantitative estimates of the scaling towards the infinite-volume.

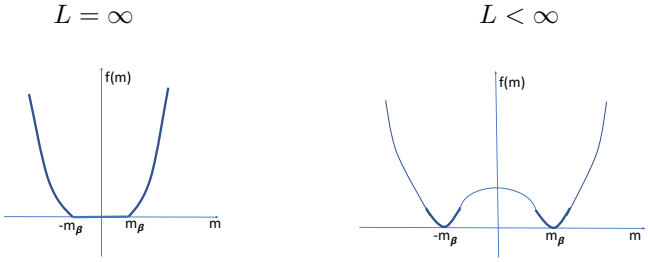

Figure 6. Schematic picture of the free energy as a function of the magnetization m, in the infinite volume ($f(m)$ left) and at finite volume ($f_L(m)$ right).

We claim that the central panel (with one bump) in Fig. 5 is a finite-size effect and it is due to the finite-volume "metastability" of the Ising model in two-dimensions. The key argument [4], from the equilibrium theory of the Ising model in $\mathbb{Z}^d$, is that f*or finite volumes stable regions are larger*: phase separation occurs at a magnetization value $m = m^*(L) < m_\beta$.

The heuristic behind this argument is recalled in Fig 6 and is explained below.

One assumes that the infinite volume free energy $f(m)$ is a convex symmetric function of the magnetization m, with $f(m) = 0$ for $m \in [-m_\beta, m_\beta]$ (left panel Fig 6); one also assumes that the finite volume free energy $f_L(\beta) = L^{-2} \log Z_L(\beta)$ has two local minima at $\pm m_\beta$ with $f_L(\pm m_\beta) = 0$ (right panel Fig 6). Under this assumptions one compares the free-energy cost of an homogeneous profile to that of a spherical droplet of radius R. This yields the equation

$$\frac{1}{2} f_L''(m_\beta)\delta^2 L^d = \tau_d R^{d-1} \tag{5.1}$$

with τ_d the surface tension. Indeed the free energy of a homogeneous profile with magnetization $m = m_\beta - \delta$ for small $\delta > 0$ is $\frac{1}{2} f_L''(m_\beta)\delta^2 L^d$, while the free energy of a spherical droplet with magnetization $-m_\beta$ in a sea of magnetization $+m_\beta$ is $\tau_d R^{d-1}$. Furthermore, imposing the constraint of a specific magnetization $m_\beta - \delta$, one has

$$(m_\beta - \delta)L^d = -m_\beta \gamma_d R^d + (L^d - \gamma_d R^d)m_\beta, \tag{5.2}$$

where in the l.h.s. we wrote the total magnetization of a homogeneous profile with magnetization $m_\beta - \delta$, and in the r.h.s. we wrote the total magnetization of a spherical droplet of radius R with magnetization $-m_\beta$ in a sea of magnetization $+m_\beta$. In the above equation $\gamma_d R^d$ with $\gamma_d = \pi^{d/2}/\Gamma(d/2+1)$ is the volume of the $d-$dimensional sphere. Working out the algebra of (5.1) and (5.2)

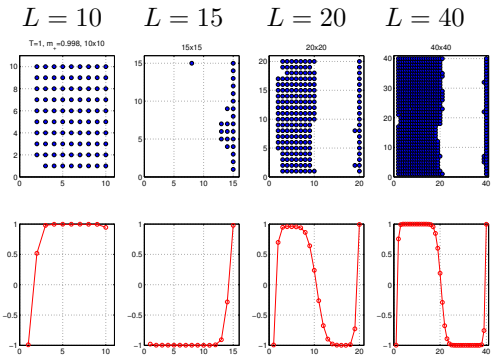

Figure 7. Stationary magnetization profiles for a sequence of increasing volumes of linear size $L = 10, 15, 20, 40$ with boundary magnetization $m_+ = 0.9990$.

one finds

$$\delta = c_d L^{-d/(d+1)}, \qquad R = c'_d L^{d/(d+1)}$$

for some constants $c_d, c'_d > 0$. Thus, in a finite volume, the homogeneous profile corresponds to a lower free energy for magnetization $m > m^*(L) = m_\beta - c_d L^{-d/(d+1)}$, and the critical droplet at $m = m^*(L)$ has radius $c'_d L^{d/(d+1)}$.

The previous argument can be turned into a rigorous theory by studying the canonical Gibbs measure conditioned to a magnetization m on the d-dimensional torus (see [4]). In $d = 2$ it implies that

- If $m \in (m_\beta - cL^{-2/3}, m_\beta)$, with $c > 0$ small enough, then the canonical Gibbs measure with magnetization m is supported by configurations with "small" contours (of size $\leq \log L$).
- If $m = m_\beta - cL^{-2/3}$ there is a droplet of size $L^{2/3}$.

We now verify indirectly that the profile with one bump is due to the finite-volume metastability. This is shown in Fig 7.

We fix the boundary magnetization to the value $m_+ = 0.9990$ $(< m_{|_{\beta=1}} = 0.99927)$ and vary the system size. Fig 7 shows the stationary magnetization profiles for a sequence of increasing volumes of linear size $L = 10, 15, 20, 40$. We see that for $L = 10$ and $L = 15$ we observe the stationary profile with one bump, either at the left boundary or at the right boundary (by symmetry they have the same probability of being observed). For the larger volumes with $L = 20$ and $L = 40$ instead we observe the profile with a double bump.

Fig. 7 is explained by the finite-volume metastability: the value $m_+ = 0.9990$ is included in the metastable region $(m_\beta - cL^{-2/3}, m_\beta)$ for $L = 10, 15$, whereas

it is unstable for $L = 20, 40$. This sustains the claim that the profile with a bump is a finite-size effect and it is due to the finite-volume "metastability" of the Ising model in two-dimensions.

6. Perspectives

The results of the numerical simulations suggest to complete the hydrodynamic picture in the low temperature regime as follows. In the unstable region $\beta > \beta_c$ and $m_+ < m_\beta$ one has:

- the current $J > 0$ (uphill diffusion);
- the stationary magnetization profile has three discontinuities: two at the boundaries (bumps) and one in the middle;
- Fick's law is safisfied, except isolated points $\{0, 1/2, 1\}$.

These properties are expected to hold for boundary magnetization value m_+ that are not too low when compared to the spontaneous magnetization m_β. For boundary magnetization m_+ substantially smaller than m_β other instabilities develop and one needs a more refined analysis, see [10].

We provided a quantitative argument suggesting that the magnetization profile with one bump are due to finite-size metastability. Thus, for $m_+ = m_\beta$, one can expect the following behavior as the system size is varied (see Figure 8):

- if one approaches the infinite volume limit by staying in the unstable region, i.e. $m_+(L) \nearrow m_\beta$ with $m_+(L) < m_\beta - cL^{-2/3}$, then one has a profile with a double bump;
- if one approaches the infinite volume limit by staying inside the metastable region, i.e. $m_+(L) \nearrow m_\beta$ with $m_+(L) > m_\beta - cL^{-2/3}$, then one has a profile with one bump;
- if one approaches the infinite volume limit from above, i.e. $m_+(L) \searrow m_\beta$ then one has the profile with one discontinuity at the middle.

It would be interesting to see if the phenomenology that has been found in the numerical simulations can be observed in real experiments. Indeed uphill diffusion is a well-known phenomenon in multi-component systems, very much studied in engineering chemistry as a way to "purify" systems, see [19–21]. The novelty predicted by our analysis is that, in the presence of a phase transition and for boundary densities inside the spinodal region, the separation of species could spontaneously occur. It is not clear however how to construct reservoirs that keep the boundary magnetization in the region $m_+ < m_\beta$.

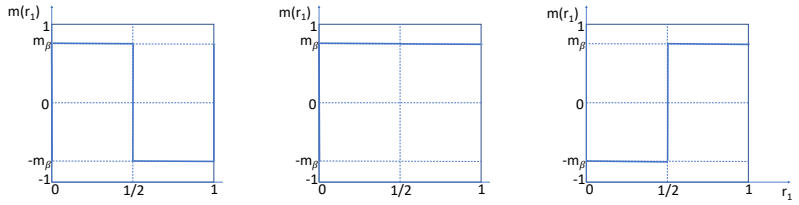

Figure 8. Stationary magnetization profile in the low temperature region for $m_+ = m_\beta$. We distinguish: $m_+(L) \nearrow m_\beta$ with $m_+(L) < m_\beta - cL^{-2/3}$ (left panel); $m_+(L) \nearrow m_\beta$ with $m_+(L) > m_\beta - cL^{-2/3}$ (central panel); $m_+(L) \searrow m_\beta$ (right panel).

Acknowledgments

I thank the organizers of the 2018 Inhomogeneous Random Systems conference. The results discussed in this paper have been obtained in collaboration with Matteo Colangeli, Claudio Giberti and Cecilia Vernia. I am in debt with Anna De Masi and Errico Presutti (GSSI) for having suggested the problem and for several discussions. I acknowledge financial support from the Italian Research Funding Agency (MIUR) through FIRB project "Stochastic processes in interacting particle systems: duality, metastability and their applications", grant n. RBFR10N90W.

References

[1] A. Iacobucci, F. Legoll, S. Olla and G. Stoltz (2011) Negative thermal conductivity of chains of rotors with mechanical forcing. *Phys. Rev. E* **84**, 061108.

[2] J.R. Baxter (2016) *Exactly Solved Models in Statistical Mechanics*. Elsevier.

[3] C. Bernardin and S. Olla (2011) Transport properties of a chain of anharmonic oscillators with random flip of velocities. *J. Stat. Phys.* **145**, 1224–1255.

[4] M. Biskup, L. Chayes and R. Kotecký (2003) Critical region for droplet formation in the two-dimensional Ising model. *Commun. Math. Phys.* **242**, 137–183.

[5] T. Bodineau and E. Presutti (2003) Surface tension and Wulff shape for a lattice model without spin flip symmetry. *Ann. H. Poincaré* **4**, 847–896.

[6] M. Colangeli, A. De Masi and E. Presutti (2016) Latent heat and the Fourier law. *Phys. Lett. A* **380**, 1710–1713.

[7] M. Colangeli, A. De Masi and E. Presutti (2017) Particle models with self sustained current. *J. Stat. Phys.* **167**, 1081–1111.

[8] M. Colangeli, A. De Masi and E. Presutti (2017) Microscopic models for uphill diffusion. *J. Phys. A: Math. Theor.* **50**, 435002.

[9] M. Colangeli, C. Giardinà, C. Giberti and C. Vernia (2018) Non-equilibrium 2D Ising model with stationary uphill diffusion. *Phys. Rev. E* **97**, 030103(R).

[10] M. Colangeli, C. Giberti, M. Kröger and C. Vernia (2019) Emergence of stationary uphill currents in 2D Ising models: the role of reservoirs and boundary conditions. *Eur. Phys. J. Spec. Top.* **228**, 69–91.

[11] L.S. Darken (1949) Diffusion of carbon in austenite with a discontinuity in composition. *Transactions of the American Institute of Mining, Metallurgical and Petroleum Engineers* **180**, 430–438.

[12] A. De Masi and E. Presutti (2006) *Mathematical Methods for Hydrodynamic Limits.* Springer.

[13] A. De Masi, E. Presutti and D. Tsagkarogiannis (2011) Fourier law, phase transitions and the stationary Stefan problem. *Archive for Rational Mechanics and Analysis* **201** (2), 681–725.

[14] R. Dobrushin, R. Kotecký and S. Shlosman (1992) *Wulff Construction: a Global Shape from Local Interaction.* Translation of Mathematical Monographs **104**, Providence, Rhode Island: American Mathematical Society.

[15] M.Z. Guo, G.C. Papanicolaou and S.R.S. Varadhan (1988) Nonlinear diffusion limit for a system with nearest neighbor interactions. *Commun. Math. Phys.* **118**, 31–59.

[16] G. Eyink, J. Lebowitz and H. Spohn (1990) Hydrodynamics of stationary non-equilibrium states for some stochastic lattice gas models. *Commun. Math. Phys.* **132**, 253–283.

[17] J. Fourier (1822) *Théorie analytique de la chaleur.* Chez Firmin Didot, père et fils.

[18] R. Krishna (2015) Uphill diffusion in multicomponent mixtures. *Chem. Soc. Rev.* **44**, 2812–2836.

[19] R. Krishna (2015) Serpentine diffusion trajectories and the ouzo effect in partially miscible ternary liquid mixtures. *Phys. Chem. Chem. Phys.* **17**, 27428.

[20] R. Krishna (2016) Highlighting diffusional coupling effects in ternary liquid extraction and comparisons with distillation. *Ind. Eng. Chem. Res.* **55**, 1053.

[21] R. Krishna (2016) Diffusing uphill with James Clerk Maxwell and Josef Stefan. *Curr. Opin. Chem. Eng.* **12**, 106–119.

[22] F. Rezakhanlou (1990) Hydrodynamic limit for a system with finite range interactions. *Commun. Math. Phys.* **129**, 445–480.

[23] L. Onsager (1944) Crystal Statistics. I. A two-dimensional model with an order-disorder transition. *Phys. Rev.* **65** (3–4), 117–149.

[24] H. Spohn (1995) Fluctuations of a flux driven interface. *Z. Phys. B* **97**, 361–365.

[25] H. Spohn and H.T. Yau (1995) Bulk diffusivity of lattice gases close to criticality. *J. Stat. Phys.* **79**, 231–241.

[26] C.N. Yang (1952) The spontaneous magnetization of a two-dimensional Ising model. *Phys. Rev.* **85**, 808–816.

[27] H.T. Yau (1991) Relative entropy and hydrodynamics of Ginzburg – Landau models. *Lett. Math. Phys.* **22**, 63–80.